Enhanced degradation of methylene blue dye using hydrothermally synthesized Nickel-doped Strontium oxide catalysts

Jehangir Shah[1], Hao Sun[2,3,4,5], Zijun Qiao[4,5], Talha Sharif[1] & Misbah Gul[1]

[1] Department of Chemistry, Abdul Wali Khan University Mardan, Mardan 23200, KP, Pakistan

[2] Faculty of Science, Autonomous University of Madrid, Spanish National Research Council (UAM-CSIC), Madrid, 28049, Spain

[3] Cantoblanco campus, Consejo Superior de Investigaciones Científicas, CSIC, Madrid, 28049, Madrid, Spain

[4] Henan Dayu Physical Agricultural Technology Research Institute, 450046, Zhengzhou, China

[5] Henan Dayu Physical Equipment Company, 450046, Zhengzhou, China

Corresponding: Hao Sun, Faculty of Science, Autonomous University of Madrid, Spanish National Research Council (UAM-CSIC), Madrid, 28049, Spain. E-mail: hao.sun01@estudiante.uam.es

Received: September 03, 2024 DOI: 10.14295/bjs.v3i12.663

Accepted: November 11, 2024 URL: https://doi.org/10.14295/bjs.v3i12.663

Abstract:

Methylene blue is an organic contaminant that is produced by the plastic, textile, and dye industries. Many studies have been undertaken to investigate the cleanup of methylene blue from industrial effluents. SrO nanoparticles are now being utilized to remove methylene blue colours from water. We used a hydrothermal technique to create strontium oxide nanoparticles for photocatalytic MB breakdown under light conditions. To enhance the solar light activity and avoid charge recombination, we employed a hydrothermal technique to add Ni as a dopant in strontium oxide nanoparticles. Strong base NaOH, nickel nitrate, and strontium nitrate were used as precursors. The nanoparticles were crushed into powder and calcined at 450 °C in a muffle furnace to produce SrO and Ni-doped SrO nanoparticles. The nanoparticles were analyzed using several analytical methods to determine their morphological and structural properties. At 309, 312, and 317 nm, UV-*Vis* spectroscopy showed absorbance values of SrO doped with varied nickel concentrations. The Ni–O stretching peak was identified in the FTIR analysis of strontium oxide nanoparticles at 402 cm^{-1} and 581 cm^{-1}, whereas the Sr–O bond gave a signal at 854.84 cm^{-1}. SEM images of Ni-doped SrO nanoparticles were created at various magnifications. The nanostrips are hexagonal and cylindrical. Sherrer's equation was used to compute the average crystalline structure, which showed that the diameters of pure and Ni-doped SrO (2 percent, 3 percent, and 4 percent) nanoparticles were 45.54 nm, 36.14 nm, 42.93 nm, and 41.21 nm, respectively. According to the EDX examination, the relative concentration of Ni-doped SrO is about 72 percent Sr and oxygen, with around 1.34 percent Ni. The resulting sample was tested for photocatalytic degradation of organic pollutants in aqueous solution, such as methylene blue, and the completion of the reaction was monitored using UV-visible spectroscopy to measure the % photocatalytic degradation during light illumination. According to the UV-visible spectra, 90% of the dye was effectively destroyed.

Keywords: degradation, methylene blue, photocatalysis, wastewater treatment, hydrothermal synthesis.

Degradação aprimorada do corante azul de metileno usando catalisadores de óxido de Estrôncio dopados com níquel sintetizados hidrotermicamente

Resumo

O azul de metileno é um contaminante orgânico produzido pelas indústrias de plástico, têxtil e corantes. Muitos estudos foram realizados para investigar a limpeza do azul de metileno de efluentes industriais. As nanopartículas de SrO agora estão sendo utilizadas para remover as cores do azul de metileno da água. Usamos uma técnica hidrotérmica para criar nanopartículas de óxido de estrôncio para quebra fotocatalítica de MB sob condições de luz. Para aumentar a atividade da luz solar e evitar a recombinação de carga, empregamos uma técnica hidrotérmica para adicionar Ni como um dopante em nanopartículas de óxido de estrôncio. NaOH de

base forte, nitrato de níquel e nitrato de estrôncio foram usados como precursores. As nanopartículas foram esmagadas em pó e calcinadas a 450 °C em um forno mufla para produzir nanopartículas de SrO e SrO dopadas com Ni. As nanopartículas foram analisadas usando vários métodos analíticos para determinar suas propriedades morfológicas e estruturais. Em 309, 312 e 317 nm, a espectroscopia UV-*Vis* mostrou valores de absorbância de SrO dopado com concentrações variadas de níquel. O pico de estiramento Ni–O foi identificado na análise FTIR de nanopartículas de óxido de estrôncio em 402 cm^{-1} e 581 cm^{-1}, enquanto a ligação Sr–O deu um sinal em 854,84 cm^{-1}. Imagens SEM de nanopartículas SrO dopadas com Ni foram criadas em várias ampliações. As nanotiras são hexagonais e cilíndricas. A equação de Sherrer foi usada para calcular a estrutura cristalina média, que mostrou que os diâmetros de nanopartículas SrO puras e dopadas com Ni (2%, 3% e 4%) eram 45,54 nm, 36,14 nm, 42,93 nm e 41,21 nm, respectivamente. De acordo com o exame EDX, a concentração relativa de SrO dopado com Ni é de cerca de 72 por cento de Sr e oxigênio, com cerca de 1,34 por cento de Ni. A amostra resultante foi testada para degradação fotocatalítica de poluentes orgânicos em solução aquosa, como azul de metileno, e a conclusão da reação foi monitorada usando espectroscopia UV-visível para medir a % de degradação fotocatalítica durante a iluminação de luz. De acordo com os espectros UV-visíveis, 90% do corante foi efetivamente destruído.

Palavras-chave: degradação, azul de metileno, fotocatálise, tratamento de águas residuais, síntese hidrotérmica.

1. Introduction

The World Health Organization (WHO) closely screens people all over the world who have access to nontoxic drinking water, with one of its key objectives being that "all human existences, regardless of whether they are adults or infants, and irrespective of their economic and social circumstances, have the complete right to have access to acceptable supply of harmless drinking water." As a result, it's critical to avoid the introduction of contaminants into the environment and to efficiently manage pollutants that have already been introduced (Madani et al., 2020).

To successfully report the usage of severe energy crises, critical environmental challenges, and fossil fuels, contemporary civilization has been looking for renewable, clean, and low-cost energy sources to exchange fossil fuels (Gupta and Tripathi, 2021). By the way, photocatalytic water splitting and photocatalytic pollutant degradation utilizing solar energy to produce hydrogen are clean and eco-friendly approaches (Leu et al., 2017). Because of their ferroelectric capabilities and small energy band gaps which allow them to absorb the bulk of visible light materials with multiferroic properties have lately been utilized for applications in both photovoltaics and photocatalysis (Zada et al., 2016; Ghani et al., 2023).

With the increase in industry and population, environmental contamination, particularly water pollution, has received a lot of attention. The generation of hydrogen on a TiO2 photoelectrode, as well as research on semiconductor photocatalysts, ushered in a new era in 1972 (Ali et al., 2019). Because of its good efficiency, simple equipment, simple handling, low energy consumption, and strong oxidation capacity, photocatalysis has been used for the photo-degradation of numerous organic contaminants (Qi et al., 2020). Photocatalysis is recognized as a cutting-edge ecologically acceptable alternative technology for degrading organic contaminants, and its implications in wastewater treatment have recently been extensively researched.

When compared to conventional physical and biological procedures, it is less expensive and easier to operate (Yadav et al., 2018; Kashif et al., 2023). Many different photocatalysts have been employed to degrade methylene blue, however, their practical applications are still limited because of low high-charge recombination rates visible-light absorption, unknown degradation, and weak surface catalysis, mechanisms (Zada et al., 2018). Stains are used in a wide range of textile and chemical industries, and they account for a significant percentage of dye utilization and wastewater emission (Worku et al., 2020; Zaman et al., 2024). Textile productions require a massive amount of water, diverse chemicals, dyes, secondary chemicals, and sizing materials in the process of fibber staining, alteration to yarn, yarn to textile, and destruction (Lee et al., 2015).

The usage of such toxic substances has damaged the environment and water. Freshwater sources/resources are dwindling as a result of extended droughts, expanding population, climate change risks, and demanding water quality regulations, leading to an increase in worldwide demand for clean water (Amin et al., 2014; Shah et al., 2024; Jamal et al., 2024). Daily, several commercial and nonprofit technical breakthroughs are used, but nanomaterials technology has shown to be one of the most sophisticated methods for wastewater treatment. Nanoscale research advancements have enabled the development of economically viable and ecologically stable treatment systems for successfully treating water/wastewater while fulfilling ever-increasing water quality requirements (Yarahmadi et al., 2021; Muhammad et al., 2023; Ahsan et al., 2024). Advances in nanotechnology

have created prospects to address future generations' fresh water needs (Savage and Diallo, 2005).

Various technologies have been devised to remove dangerous contaminants from the environment, particularly wastewater from various businesses. Coagulation, Adsorption, calcination, filtration, advanced oxidation, and other techniques have been used to remove undesirable contaminants from wastewater (Zada et al., 2021; Muhammad et al., 2023; Niaz et al., 2024; Kashif et al., 2024a). Though many of these approaches are quite successful, they are not universal since one method can be utilized for some contaminants but not for others. These technologies necessitate costly operating strategies as well as the generation of additional pollutants, some of which are considerably more harmful than the original pollutants (Xu et al., 2019).

As a result, improved approaches must be developed and used to successfully combat these contaminants (Zada et al., 2021). Various technologies have been devised to remove dangerous contaminants from the environment, particularly wastewater from various businesses. Adsorption, coagulation, filtration, calcination, advanced oxidation, and other techniques have been used to remove undesirable contaminants from wastewater (Ali et al., 2019). Photocatalysis discusses the use of a catalyst to speed up a photo process. The following summarizes the entire process of semiconductor-sensitized photoreactions:

$$A + D \xrightarrow[\text{Light}]{\text{Semoconductor}} A^- + D^+$$

The absorption of a photon of light having an energy band gap activates the semiconductor photocatalysts, resulting in the excitation of electrons from the valence band to the conduction band while leaving holes in the valence band (Gupta and Tripathi, 2021). The primary criteria for effective photocatalysts are that the plentiful interfacial electron processes that involve that hole and electron must compete effectively with the main deactivation mechanisms involving electron-hole recombination (Gupta and Tripathi, 2021).

Nanoparticles have easily penetrate extensively into the water/wastewater network and treat it in ways that standard technologies cannot. The enhanced surface-to-volume ratio of nanoparticles increases their interaction with environmental pollutants (Raziq et al., 2022). When nanoparticles with absorptions, interfacial, and reaction capacities engage with aqueous systems, they can behave like colloids or exhibit quantum-size effects. They can save energy and money because of their modest size (Shah et al., 2024; Kashif et al 2024b; Kashif et al., 2024c).

Because of their high removal effectiveness in degrading and mineralizing organic contaminants from water, advanced oxidation processes, and photocatalysis processes have sparked increased attention in the field of water treatment (Khan et al., 2020). Meanwhile, AOPs and photocatalysis processes are more ecologically friendly than other treatment methods, such as physical and chemical techniques, since AOPs and photocatalysis processes do not produce harmful residues or change organic pollutants from one phase to another (Xiong et al., 2022).

2. Material and Methods

2.1 Ni-doped production

For the preparation of Ni-doped SrO samples, $Ni(NO_3)_2$ and strong base NaOH were applied as the precursor salts of Ni^{2+} and $Sr(NO_3)_2 \cdot 6H_2O$ as the source of strontium while deionized water was used as a solvent. The hydrothermal approach was used to synthesize Strontium oxide nanoparticles. 4g of Strontium nitrate hexahydrate was dissolved in 60 mL deionized water while a nickel nitrate solution was made and added to three distinct strontium nitrate solutions. The combination was continually agitated at room temperature to generate a homogenous mixture.

The solution pH was kept constant at 9 by adding 10% sodium hydroxide solution to the above-mentioned homogenous combination. A white precipitate was formed. The precipitate was resolved to get a homogenous solution. The homogenous solution was then placed in a Teflon stainless steel autoclave in a 180 ºC oven for 12 hours to get the precipitate under high temperature and pressure. Once the autoclave had cooled, the precipitate was washed and centrifuged to eliminate unreacted reactants. To make Ni-doped strontium oxide nanoparticles, the precipitate was dried in an oven at 100 °C and calcined for 1 h at 450 °C, as shown in (Figure 1).

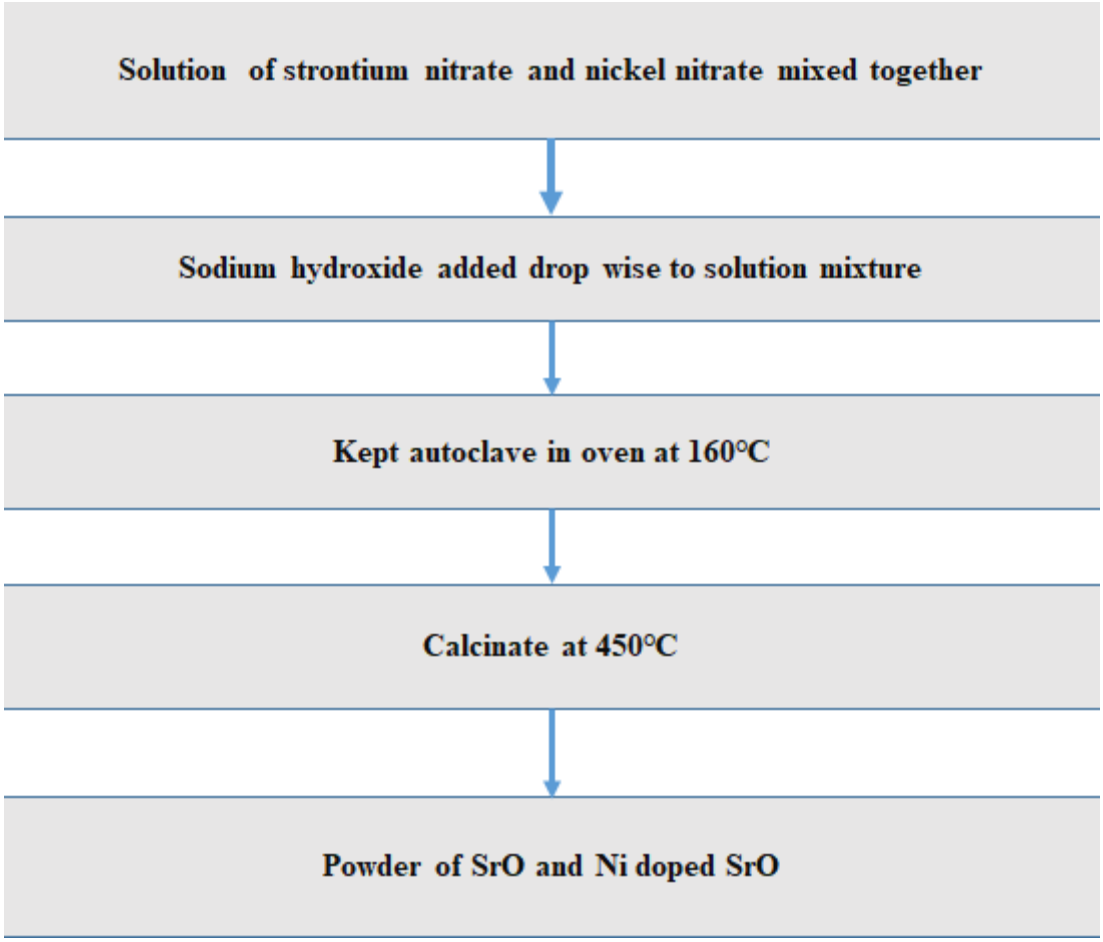

Source: Authors, 2024.

2.2 Characterization

The SP-300 dual beam spectro-photometer was utilized to record the highest absorption and optimize generated NPs. The researchers used a single beam optical detector from Japan with a bandwidth of 1nm and a spectrum was recorded of 190 to 1100 nm. The technique was developed in the chemistry department at Bacha Khan University KPk in Pakistan, and it used wavelengths ranging from 200 nm to 800 nm. FTIR spectra were used to characterize the functional groups of SrO NPs (Hall et al., 2007). A 0.05g sample was taken, put in a sample cell, and then compressed to create the spectrum.

The Department of Chemistry at BKUC KPK in Pakistan led spectra between 4000 and 400 cm^{-1} (100 outputs). Strontium Oxide NPs' crystal-like structure will be investigated. Drops of Strontium Oxide NPs produced from strontium nitrate were placed on the glass for X-ray diffraction at the SNS, NUST Islamabad, Pakistan, and also the Diffractometer apparatus was maintained running at a current of 20 milliamperes and a voltage of 40 kilovolts, with Cu K radiation being used in addition. SEM analysis was utilized to assess the size and shape of SrO NPs. A 15-kV acceleration voltage generated scanning electron microscopy (SEM) pictures. Micrographs are magnified 100-5000 times (Kumar et al., 2017).

The following settings were determined to be ideal. Contact with the beam: Signal SE1, 20–21 mm working distance, spot size 40 nm, 20–21 mm working distance for elemental constituent assurance, and an EDX technique for SrO NPs was used electron thumps on the surface of the sample beam. The energy range of the beam is 0-14 Kev. X-rays were created by the irradiated substance. The sample under consideration determines the energy of the emitted X-rays. At a depth of 2, X-rays were generated. Using a circulating electron ray on the sample, a 2D picture of each constituent in the sample may then be generated (Akbari et al., 2011).

2.3 *Photocatalysis of methylene blue dye*

For degradation, methylene blue dye was used to measure the photocatalytic effectiveness of the acquired samples. The photocatalysis was carried out utilizing an incandescent light bulb (100 volts). In 100 mL of 10 ppm methylene blue solution, 0.2 g photocatalysts were scattered. The previously mentioned suspension was agitated in the dark for 30 min to attain an adsorption/desorption equilibrium. The mixture was then exposed while being vigorously stirred 10 mL of this solution was taken and centrifuged regularly to remove the solid photocatalyst. Finally, the adsorption of dye and degradation efficiency of the photocatalyst were evaluated using UV-visible spectrometry. The dye clearance percentage was estimated using (Equation 1).

$$\text{Degradation efficiency (\%)} = C_0 - C_t/C_0 \times 100 \quad (1)$$

Where: C_0 is the initial concentration of methylene blue while C_t is the concentration at time t.

3. Results

The morphological, visual features, and structural, of improved Ni\SrO were investigated utilizing a variety of approaches in this study. The photocatalytic degradation of produced photocatalysts was then evaluated using the degradation of MB dye under light**.**

3.1 UV-Visible spectroscopy

UV-visible is a quick, cheap, and easy characterization approach extensively employed in Nano Materials studies. Because the optical characteristics of certain metal nanomaterials are thoughtful to size, shape, concentration, aggregation state, and refractive index closer to the surface, UV-visible spectroscopy is a helpful method for characterizing them (Davydov and Sheppard, 2003). The UV-visible spectra of SrO and Ni-doped SrO Nps were measured from 200 to 800 nm, and the UV-*Vis* spectra of SrO and Ni/SrO nanoparticles were measured.

Figure 3.1 displays a broad wide excitonic absorption band at 295 nm with a band gap of roughly 4.1 eV. The absorption edges are gradually expanded to longer wavelength regions after Ni doping to reduce band gaps. Interestingly 2, 3, and 4Ni/SrO nano size crystals show absorption boundaries at 309, 312, and 317 nm, respectively (Li et al., 2016). The Tauc plot was used to calculate the optical energy band gaps (Humayun et al., 2016). The pure, 2%, 3%, and 4% band gaps Nanocrystals of Ni-doped SrO are 4.2, 4, 3.97, and 3.91 eV, respectively, based on absorption spectra as shown in (Figure 3.1). Based on these results, it is obvious that as the amount of Ni increases, the band gap energies decrease slowly, which has a significant impact on the photocatalytic activity of SrO nanoparticles (Xu et al., 2019).

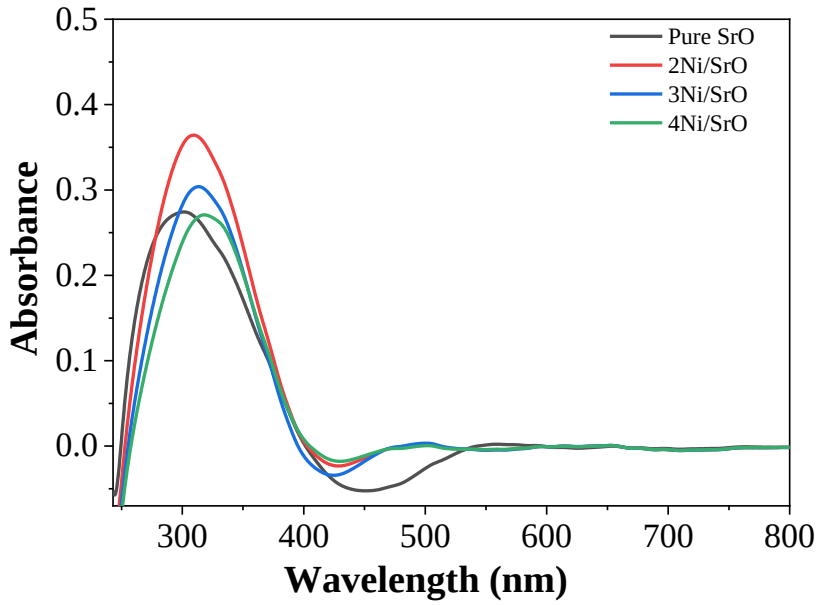

Figure 3.1. UV-visible spectra of strontium oxide 2%, 3%, and 4% Ni-doped strontium oxide nanoparticle. Source: Authors, 2024.

3.2 Fourier transform infrared spectroscopy (FTIR) spectrum

FTIR method is utilized to classify various functional groups in materials. Because the strength of the FTIR peak is a significant indication of the type of constituents present, it is an excellent instrument for qualitative research (Athar, 2013). Figure 3.3 depicts the FTIR spectrum recorded between 4000 and 400 cm^{-1}. The maximum of Ni–O–H bending vibrations and Ni–O stretching may be seen at approximately 405 cm^{-1} and 582 cm^{-1}, respectively (Budipramana et al., 2014). The indication at 854.84 cm^{-1} in the FTIR spectra of strontium oxide nanoparticles is caused by Sr–O stretching (Ghani et al., 2023). The H-O-H bending has significant peaks at 1435.77 cm^{-1} and 1770.29 cm^{-1}, as illustrated in (Figure 3.3). The peak at 3000-3600 cm^{-1} represents the –OH group and interstitial water molecules (Jing et al., 2012).

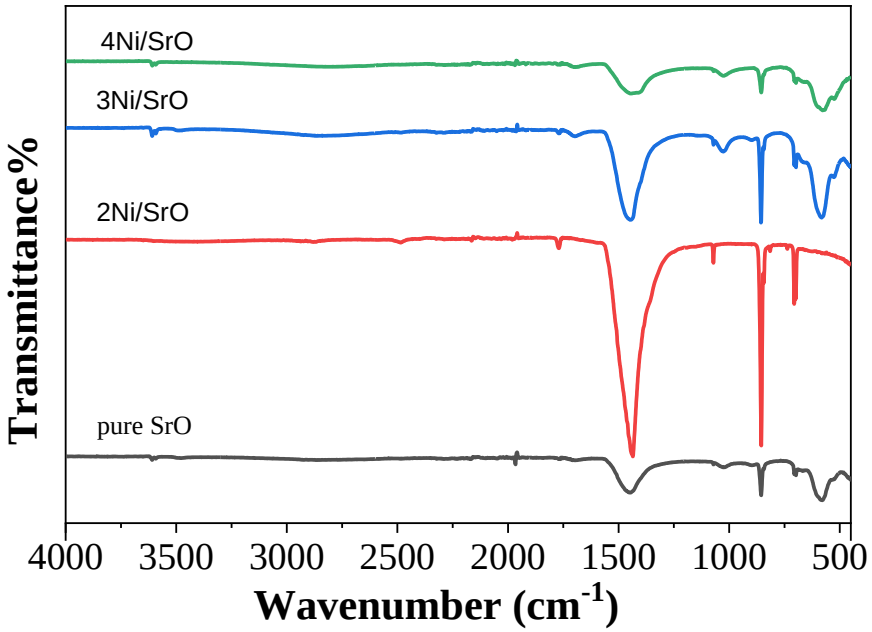

Figure 3.2. FTIR spectra of strontium and 2Ni, 3Ni, and 4Ni doped strontium oxide nanoparticles. Source: Authors, 2024.

3.3 X-ray diffraction (XRD)

XRD is an operative nondestructive method for characterizing nanocrystals (Larquet and Carenco, 2020). It's utilized to calculate structures, phases, preferred crystalline structure (texture), and other structural information like mean particle size, strain, crystalline nature, and crystal deficiencies. Figure 3.2 depicts the XRD results from our sample (Rabeie et al., 2022). Pure SrO has nine distinct and strong XRD peaks at 2 = 14, 19, 24, 25, 28, 31, 35, 36, and 39°, which correspond to crystal planes (101), (112), (200), (202), (114), (213), (222), (310), and (312), respectively (Sakar et al., 2013).

These XRD peaks are very narrow and crispy, specifying that the samples are very highly crystalline materials (indicates the decent crystallinity of the Strontium oxide samples). Interestingly, the inclusion of Ni as a dopant promotes the formation of (202) and (310) crystal planes, while the strength of the XRD peak at 19° has been greatly enhanced (Oskam, 2006). The average crystallite diameters of pure, 2%, 3%, and 4Ni/SrO nanoparticles were determined in this study to be 45 nm, 36nm, 43 nm, and 41nm, respectively. All samples are roughly the same size, with no discernible peak change in the XRD pattern. Furthermore, when the quantity of nickel dopant increases, so does the XRD peak intensity (Zada et al., 2020) as clearly shown in (Figure 3.2).

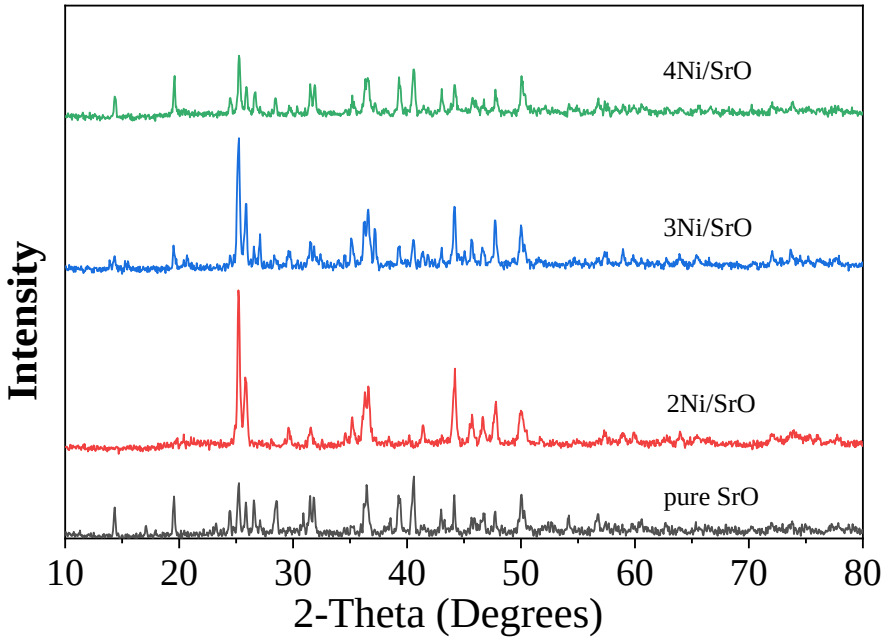

Figure 3.3. XRD pattern of strontium and 2Ni, 3Ni, 4Ni/SrO. Source: Authors, 2024.

3.4 Scanning electronic microscopy (SEM)

SEM pictures of Ni-doped SrO nanoparticles at diverse magnifications are shown in Figure 3.4 (a, b, c). The SEM images reveal that the nanostrips with lower Ni dopant concentrations had a smooth surface. Particles of various sizes are observed with cubical and cylindrical morphologies. Furthermore, when the concentration of Ni dopant increases, a significant reduction in agglomeration is seen.

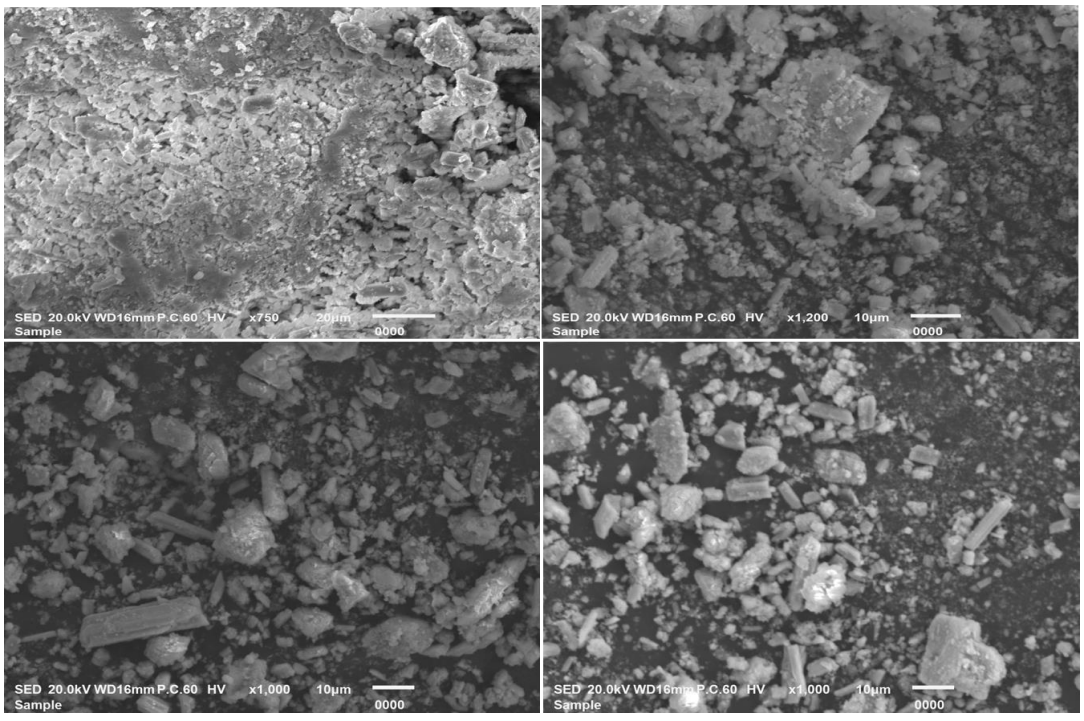

Figure 3.4. SEM images of Ni-doped strontium oxide. Source: Authors, 2024.

3.5. Energy dispersive X-Ray (EDX)

The fundamental compositions of samples are as small as limited cubic micrometers and are commonly identified and analyzed using the EDX technique. The EDX data and elemental composition of the 2Ni/SrO sample are shown in (Figure 3.5). All the essential elements are present in the samples indicating the high purity of the samples. Also, strontium and oxygen are present in a high amount while the doped Ni is about 1.34% in the sample 2Ni/SrO.

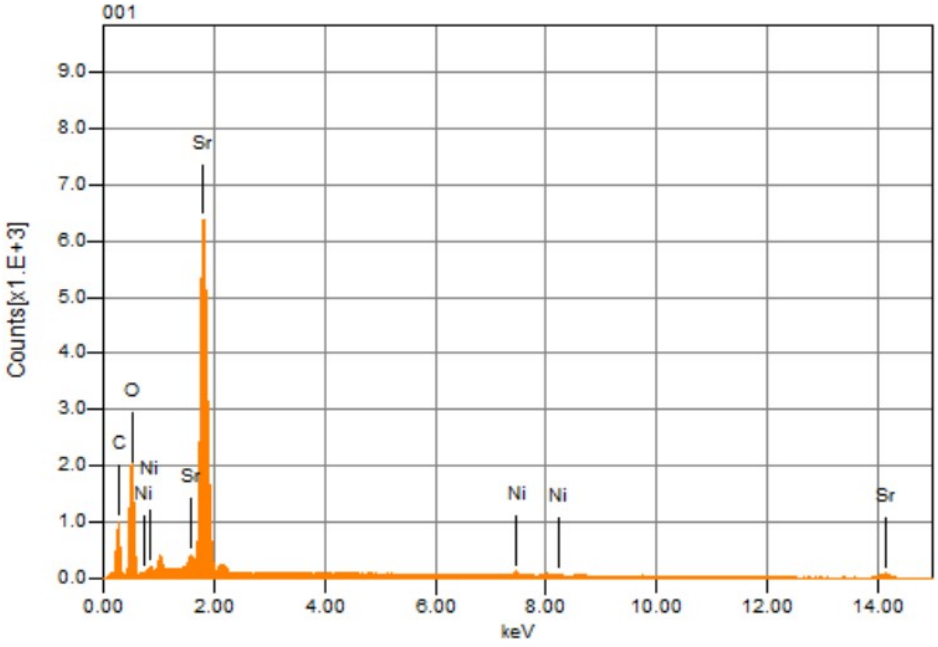

Formula	mass%	Atom%	Sigma	Net	K ratio	Line
C	26.62	45.63	0.04	25355	0.0031980	K
O	35.16	45.24	0.10	53966	0.0311058	K
Ni	1.34	0.47	0.04	5061	0.0042814	K
Sr	36.89	8.67	0.16	359046	0.1156160	L
Total	100.00	100.00				

Figure 3.5. EDX of Ni-doped strontium oxide. Source: Authors, 2024.

4. Discussion

4.1 Photocatalytic degradation

The photocatalytic activity of a semiconductor is triggered by absorbing light energy equal to or higher than its band gap energy, which leads to the formation of excited electrons and holes. When adsorbed reactants travel to the surface, the electron-hole pair interacts with them, boosting the reduction and oxidation processes. The photocatalytic activity of SrO and Ni-doped SrO nanoparticles was appraised using the degradation of MB under visible-light irradiation at room temperature. The photocatalysts were added to a 5 mg L^{-1} methylene blue solution at a concentration of 0.2 g 100 mL^{-1} (MB).

The mixture was magnetically agitated in the dark for 30 minutes to achieve adsorption-desorption equilibrium between the MB dye and the photocatalyst surface (Yasmeen et al., 2019). The mixture was subjected to visible irradiation employing Tungsten filament light at a distance of three. The reaction mixture was continually agitated, with 10 mL aliquots taken every 30 min and centrifuged for 5 min at 2000 rpm, as illustrated in (Figure 4.1). Because of its large band gap and quick charge recombination, pure SrO has comparatively modest photocatalytic activity.

However, when Ni is added as a dopant, the photocatalytic activity significantly rises. Furthermore, as the quantity of Ni dopant increases, so does the photocatalytic degradation, with the 3Ni/SrO sample demonstrating the maximum degradation efficiency. However, increasing the proportion of Ni (4Ni/SrO) reduces photocatalytic activity, which is due to the shadow effect of Ni. The photocatalytic degradation of methylene shows that Ni is

crucial in prolonging light absorption and minimizing charge recombination in SrO nanoparticles.

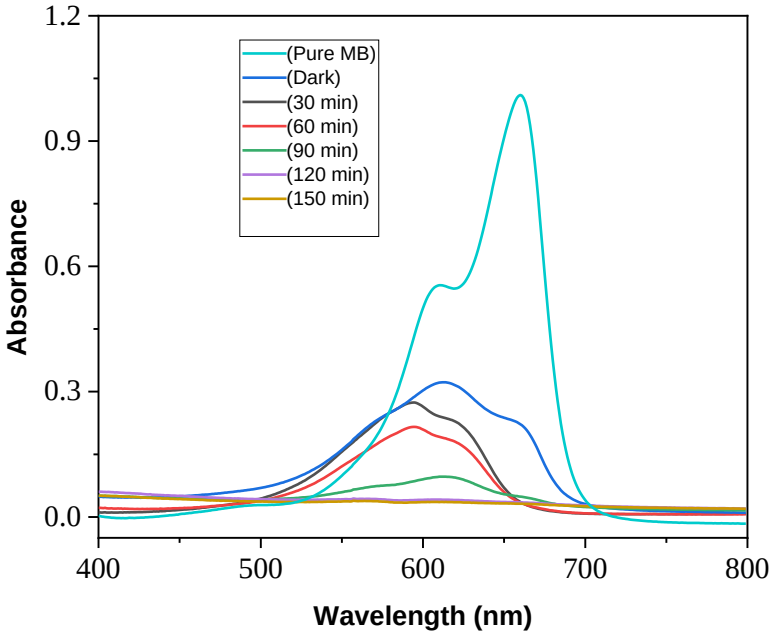

Figure 4.1 (a). Photocatalytic degradation of MB using SrO nanoparticles. Source: Authors, 2024.

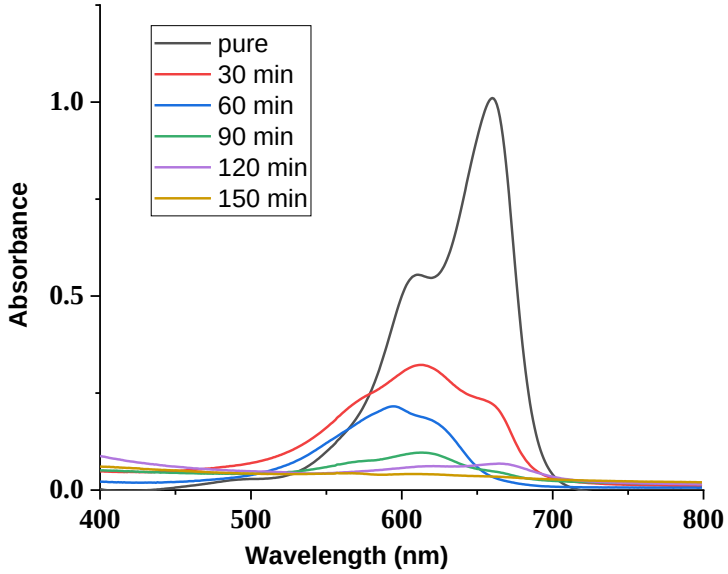

Figure 4.1 (b). Photocatalytic degradation of MB using 2Ni\Sro nanoparticles. Source: Authors, 2024.

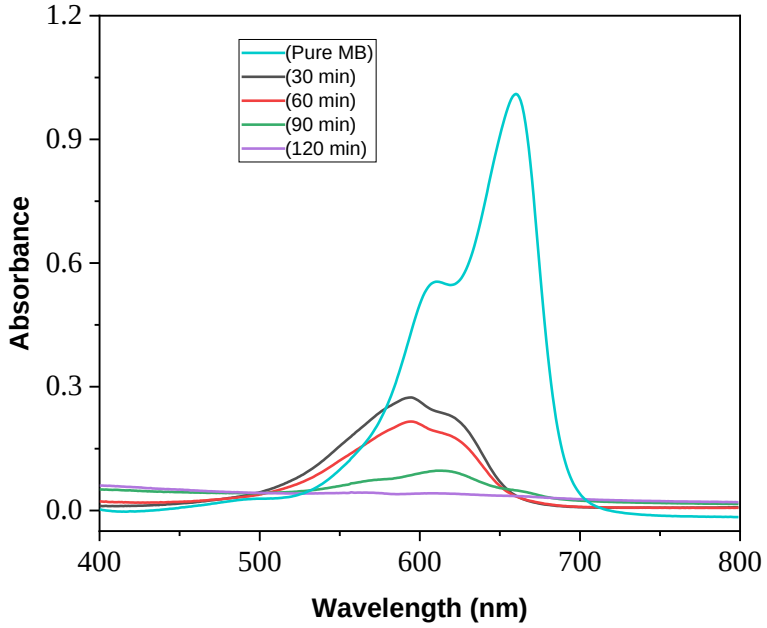

Figure 4.1 (c). Photocatalytic degradation of MB using 3Ni/SrO nanoparticles. Source: Authors, 2024.

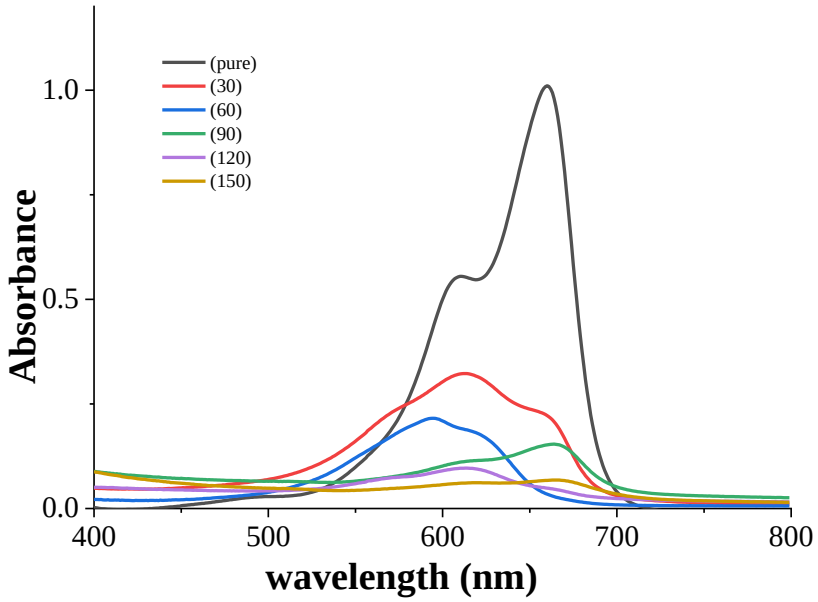

Figure 4.1 (d). UV visible photocatalytic degradation of MB using 4Ni/SrO nanoparticle. Source: Authors, 2024.

Table 1. Percent degradation.

Time	**Percent degradation**			
(min)	**Pure SrO**	**2Ni/SrO**	**3Ni/SrO**	**4Ni/SrO**
0	2	2	4	2
30	15	15	27	14
60	38	38	77	33
90	72	75	87	71
120	83	85	89	81
150	87	88	-------	84

Source: Authors, 2024.

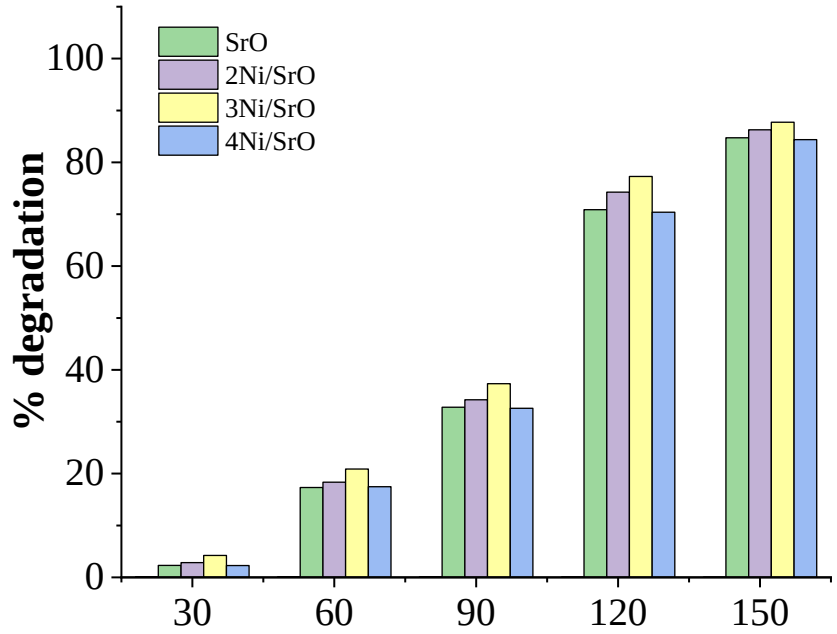

Figure 4.1 (e). %photocatalytic degradation by SrO and 2, 3, 4Ni/doped SrO. Source: Authors, 2024.

5. Conclusion

Using strontium nitrate, nickel nitrate, and sodium hydroxide as precursor materials, we effectively synthesized strontium oxide and Ni-doped strontium oxide nanoparticles by hydrothermal technique. After surface contaminants are eliminated, the crystallite size rises with calcination temperature owing to the self-assembly of nanoscale materials inside. Strontium oxide nanoparticles are metallic nanoparticles that are fewer than 100 nm in size.

It possesses good oxidation chemical inertness, resistance, and attractive characteristics. As-prepared samples were examined for phase purity, optical properties, and morphology using UV-*Vis*, FTIR, XRD, SEM, and EDX. The crystalline nature of the generated systems was shown by XRD analysis. The usual patterns of vibration in strontium oxide nanostructures were determined using FTIR spectrum analysis. The optical properties of SrO and NiSrO were investigated using UV-visible spectra. To evaluate the photocatalytic activity of strontium and Ni-doped strontium oxide-generated photocatalysts, methylene blue was employed as a model pollutant. Ni-doped strontium oxide photocatalysts degraded more than 90% of the methylene blue dye, while strontium oxide nanoparticles degraded approximately 85%.

6. Acknowledgement

The author greatly acknowledges the Department of Chemistry, Abdul Wali Khan University for providing experimental facilities.

7. Authors Contribution

Jehangir Shah: Conceptualization, methodology, investigation, writing—original draft preparation. *Hao Sun*: Supervision, funding acquisition, writing & editing, project administration. *Talha Sharif*: Data curation, formal analysis, validation. *Misbah Gul*: Conceptualization, writing - review & editing. *Zijun Qiao*: Conceptualization, writing - review & editing.

8. Conflicts of Interest

No conflict of interest.

9. Ethics Approval

Not applicable.

10. References

Ahsan, M., Qasim, S., Shah, A., Nawaz, I., Kashif, M., & Ahmad, W. J. B. J. O. S. (2024). Loading of anticancer drug anastrozole using Fe_3O_4@ SiO_2. *Brazilian Journal of Science*, 3(2), 93-101. https://doi.org/10.14295/bjs.v3i2.497

Akbari, B., Tavandashti, M. P., Zandrahimi, M. J. I. J. o. M. S., & Engineering. (2011). Particle size characterization of nanoparticles–a practical approach. *Iranian Journal of Materials Science & Engineering*, 8(2), 48-56. https://inis.iaea.org/search/search.aspx?orig_q=RN:43049756

Ali, N., Zada, A., Zahid, M., Ismail, A., Rafiq, M., Riaz, A., & Khan, A. J. J. o. t. C. C. S. (2019). Enhanced photodegradation of methylene blue with alkaline and transition-metal ferrite nanophotocatalysts under direct sun light irradiation. *Journal of the Chinese Chemical Society*, 66(4), 402-408. https://doi.org/10.1002/jccs.201800213

Ali, S., Li, Z., Chen, S., Zada, A., Khan, I., Khan, I., Ali, W., Shaheen, S., Qu, Y., & Jing, L. (2019). Synthesis of activated carbon-supported TiO2-based nano-photocatalysts with well recycling for efficiently degrading high-concentration pollutants. *Catalysis Today*, 335, 557-564. https://doi.org/10.1016/j.cattod.2019.03.044

Amin, M. T., Alazba, A. A., Manzoor, U. (2014). A review of removal of pollutants from water/wastewater using different types of nanomaterials. *Advances in Materials Science and Engineering*, (1), 825910. https://doi.org/10.1155/2014/825910

Athar, T. J. M. F. (2013). Synthesis and characterization of strontium oxide nanoparticles via wet process. *Materials Focus*, 2(6), 450-453. https://www.ingentaconnect.com/contentone/asp/mf/2013/00000002/00000006/art00004

Budipramana, Y., Ersam, T., & Kurniawan, F. (2014). Synthesis nickel hydroxide by electrolysis at high voltage. *ARPN Journal of Engineering and Applied Sciences*, 9(11), 2074-2077. http://www.scopus.com/inward/record.url?scp=84911975219&partnerID=8YFLogxK

Davydov, A. A., & Sheppard, N. (2003). Molecular spectroscopy of oxide catalyst surfaces (Vol. 690): Wiley Chichester. https://doi.org/10.1002/0470867981

Ghani, I., Kashif, M., Khattak, O. A., Shah, M., Nawaz, S., Ullah, S., Murad, S., Naz, S., Khan, H. W., Muhammad, S. & Jamal, M. (2023). Hydrothermal synthesis and characterization of Cobalt doped Bismuth oxide NPs for photocatalytic degradation of methyl orange dye. *Journal of Xi'an Shiyou University, Natural Science Edition*, 19(7), 1195-1217. https://www.xisdxjxsu.asia/viewarticle.php?aid=2506

Gupta, S. M., & Tripathi, M. (2012). An overview of commonly used semiconductor nanoparticles in photocatalysis. *High Energy Chemistry*, 46, 1-9. https://doi.org/10.1134/S0018143912010134

Hall, J. B., Dobrovolskaia, M. A., Patri, A. K., & McNeil, S. E. (2007). Characterization of nanoparticles for therapeutics. *Nanomedicine*, 2(6), 789-803. https://doi.org/10.2217/17435889.2.6.789

Humayun, M., Zada, A., Li, Z., Xie, M., Zhang, X., Qu, Y., Raziq, F., & Jing, L. (2016). Enhanced visible-light activities of porous $BiFeO_3$ by coupling with nanocrystalline TiO_2 and mechanism. *Applied Catalysis B: Environmental*, 180, 219-226. https://doi.org/10.1016/j.apcatb.2015.06.035

Jamal, M., Nabi, G. A. K., Sun, H., Ullah, K., Khattak, O. A., Kashif, M., Khan, S., Alam, M., Hussain, S., Ullah, M., Aleena, S., Haq, H., Umar, S., Atif, M., Hussain, I., & Masood, A. (2024). Preparation of Manganese-Doped Bismuth Oxide for the Photocatalytic Degradation of Methylene Blue. *Archives of Advanced Engineering Science*, 1-8. https://doi.org/10.47852/bonviewAAES42023402

Jing, L., Qin, X., Luan, Y., Qu, Y., & Xie, M. (2012). Synthesis of efficient TiO2-based photocatalysts by phosphate surface modification and the activity-enhanced mechanisms. *Applied Surface Science*, 258(8), 3340-3349. https://doi.org/10.1016/j.apsusc.2011.07.101

Kashif, M., Ali, M., Naz, S., Amir, J., Murad, S., Atif, M., Khattak, O. A., Ukkah, S., Aleena, S., Khan, N. & Khan, M. Y. (2024a). Formulation development and characterization of quercetin loaded poly caprolactone nanoparticles for tumors. *Brazilian Journal of Science*, 3(2), 82-92. https://doi.org/10.14295/bjs.v3i2.494

Kashif, M., Jawad, M., Khan, A. A., Sun, H., Ullah, K., Fakayode, O., & Azizi, S. (2024b). Fe/Ti-codoped strontium oxide nanoparticles for enhanced photocatalytic degradation of methyl orange. *Journal of Applied Research in Water and Wastewater*, 11(1), 8-14. https://doi.org/10.22126/arww.2024.10753.1336

Kashif, M., Khan, A. A., Sun, H., Kamal, J., Shah, M. I. A., Hussain, S., Amir, J., Jamal, Y., & Ahmad, T. (2024c). Synthesis and characterization of Fe-doped CuO nanoparticles: Catalytic efficiency in crystal violet dye degradation and exploration of electrical properties. *Brazilian Journal of Science*, 3(8), 1-18. https://doi.org/10.14295/bjs.v3i8.601

Kashif, M., Muhammad, S., Ali, A., Ali, K., Khan, S., Zahoor, S., & Hamza, M. J(2023). Bismuth oxide nanoparticle fabrication and characterization for photocatalytic bromophenol blue degradation. *Journal of Xi'an Shiyou University, Natural Science Edition*, 19(07), 521-544. https://www.xisdxjxsu.asia/viewarticle.php?aid=2457

Khan, M., Hayat, A., Mane, S. K. B., Li, T., Shaishta, N., Alei, D., Zhao, T. K., Ullah, A., Zada, A., Rehman, A., & Khan, W. U. (2020). Functionalized nano diamond composites for photocatalytic hydrogen evolution and effective pollutant degradation. *International Journal of Hydrogen Energy*, 45(53), 29070-29081. https://doi.org/10.1016/j.ijhydene.2020.07.274

Kumar, A., & Dixit, C. K. (2017). Methods for characterization of nanoparticles. In Advances in nanomedicine for the delivery of therapeutic nucleic acids (pp. 43-58): Elsevier. https://doi.org/10.1016/B978-0-08-100557-6.00003-1

Larquet, C., & Carenco, S. (2020). Metal oxysulfides: from bulk compounds to nanomaterials. *Frontiers in Chemistry*, 8, 179. https://doi.org/10.3389/fchem.2020.00179

Lee, H., Park, Y.-K., Kim, S.-J., Kim, B.-H., & Jung, S.-C. (2015). Titanium dioxide modification with cobalt oxide nanoparticles for photocatalysis. *Journal of Industrial and Engineering Chemistry*, 32, 259-263. https://doi.org/10.1016/j.jiec.2015.08.025

Li, F., Wangyang, P., Zada, A., Humayun, M., Wang, B., & Qu, Y. (2016). Synthesis of hierarchical Mn_2O_3 microspheres for photocatalytic hydrogen production. *Materials Research Bulletin*, 84, 99-104. https://doi.org/10.1016/j.materresbull.2016.07.032

Liu, L., Zhang, X., Yang, L., Ren, L., Wang, D., & Ye, J. (2017). Metal nanoparticles induced photocatalysis. *National Science Review*, 4(5), 761-780. https://doi.org/10.1093/nsr/nwx019

Madani, S. S., Habibi-Yangjeh, A., Asadzadeh-Khaneghah, S., Chand, H., Krishnan, V., & Zada, A. (2021). Integration of $Bi_4O_5I_2$ nanoparticles with ZnO: impressive visible-light-induced systems for elimination of aqueous contaminants. *Journal of the Taiwan Institute of Chemical Engineers*, 119, 177-186. https://doi.org/10.1016/j.jtice.2021.01.020

Muhammad, S., Ali, A., Shah, J., Hamza, M., Kashif, M., Khel, B. K. A., & Iqbal, A. (2023). Using *Moringa oleifera* stem extract for green synthesis, characterization, and anti-inflammatory activity of silver oxide nanoparticles. *Natural and Applied Sciences International Journal (NASIJ)*, 4(1), 80-97. https://doi.org/10.47264/idea.nasij/4.1.6

Muhammad, S., Ali, A., Zahoor, S., Xinghua, X., Shah, J., Hamza, M., . . . Iqbal, A. J. A. S. A. P. V. (2023). Synthesis of Silver oxide nanoparticles and its antimicrobial, anticancer, anti-inflammatory, wound healing, and immunomodulatory activities - A review. *Acta Scientific Applied Physics*, 3(7). https://www.actascientific.com/ASAP/ASAP-03-0140.php

Niaz, M., Abrar, H., Ashfaq, S., Khan, N., Awais, M., e Baseerat, N., Jadoon, R., Abrar, A., Kashif, M., & Ullah, K. (2024). Qualitative phytochemical analysis and *in vitro* antibacterial activity of *Punica granatum*. *Phytopharmacology Research Journal*, 3(1), 31-38. https://www.ojs.prjn.org/index.php/prjn/article/view/64

Oskam, G. (2006). Metal oxide nanoparticles: synthesis, characterization and application. *Journal of Sol-Gel Science and Technology*, 37, 161-164. https://doi.org/10.1007/s10971-005-6621-2

Qi, K., Xing, X., Zada, A., Li, M., Wang, Q., Liu, S.-Y., Lin, H., & Wang, G. J. C. I. (2020). Transition metal doped ZnO nanoparticles with enhanced photocatalytic and antibacterial performances: experimental and DFT studies. *Ceramics International*, 46(2), 1494-1502. https://doi.org/10.1016/j.ceramint.2019.09.116

Rabeie, B., Mahmoodi, N. M., & Mahkam, M. (2022). Morphological diversity effect of graphene quantum dot/MIL88A (Fe) composites on dye and pharmaceuticals (tetracycline and doxycycline) removal. *Journal of Environmental Chemical Engineering*, 10(5), 108321. https://doi.org/10.1016/j.jece.2022.108321

Raziq, F., Aligayev, A., Shen, H., Ali, S., Shah, R., Ali, S., Bakhtiar, S. H., Ali, A., Zarshad, N., Zada, A., Xia, X., Zu, X., Khan, M., Wu, X., & Kong, Q. (2022). Exceptional photocatalytic activities of rGO modified (B, N) Co-doped WO3, coupled with CdSe QDs for one photon Z-scheme system: a joint experimental and dft study. *Advanced Science*, 9(2), 2102530. https://doi.org/10.1002/advs.202102530

Sakar, M., Balakumar, S., Saravanan, P., & Jaisankar, S. N. (2013). Annealing temperature mediated physical properties of bismuth ferrite ($BiFeO_3$) nanostructures synthesized by a novel wet chemical method. *Materials Research Bulletin*, 48(8), 2878-2885. https://doi.org/10.1016/j.materresbull.2013.04.008

Savage, N., & Diallo, M. S. (2005). Nanomaterials and water purification: opportunities and challenges. *Journal of Nanoparticle Research*, 7, 331-342. https://doi.org/10.1007/s11051-005-7523-5

Shah, M., Hameed, A., Kashif, M., Majeed, N., Muhammad, J., Shah, N., Rehan, T., Khan, A., Uddin, J., Khan, A., & Kashtoh, H. (2024). Advances in agar-based composites: a comprehensive review. *Carbohydrate Polymers*, 346, 122619. https://doi.org/10.1016/j.carbpol.2024.122619

Worku, A., Ayele, D., & Habtu, N. (2020). Recent advances and future perspectives in engineering of bifunctional electrocatalysts for rechargeable zinc – air batteries. *Materials Today Advances*, 9, 100116. https://doi.org/10.1016/j.mtadv.2020.100116

Xiong, X., Zhang, Y., Wang, L., & Tsang, D. C. W. (2022). Chapter 1 - Overview of hazardous waste treatment and stabilization/solidification technology, in Low Carbon Stabilization and Solidification of Hazardous Wastes, Elsevier, 1-14. https://doi.org/10.1016/B978-0-12-824004-5.00031-1

Xu, B., Zada, A., Wang, G., Qu, Y. (2019). Boosting the visible-light photoactivities of $BiVO_4$ nanoplates by Eu doping and coupling CeO x nanoparticles for CO_2 reduction and organic oxidation. *Sustainable Energy & Fuels*, 3(12), 3363-3369. https://doi.org/10.1039/C9SE00409B

Yadav, N., Chaudhary, L., Sakhare, P., Dongale, T., Patil, P., Sheikh, A. D. (2018). Impact of collected sunlight on $ZnFe_2O_4$ nanoparticles for photocatalytic application. *Journal of Colloid and Interface Science*, 527, 289-297. https://doi.org/10.1016/j.jcis.2018.05.051

Yarahmadi, M., Maleki-Ghaleh, H., Mehr, M. E., Dargahi, Z., Rasouli, F., & Siadati, M. H. (2021). Synthesis and characterization of Sr-doped ZnO nanoparticles for photocatalytic applications. *Journal of Alloys and Compounds*, 853, 157000. https://doi.org/10.1016/j.jallcom.2020.157000

Yasmeen, H., Zada, A., Li, W., Xu, M., & Liu, S. (2019). Suitable energy platform of Bi_2WO_6 significantly improves visible-light degradation activity of g-C_3N_4 for highly toxic diuron pollutant. *Materials Science in Semiconductor Processing*, 102, 104598. https://doi.org/10.1016/j.mssp.2019.104598

Zada, A., Humayun, M., Raziq, F., Zhang, X., Qu, Y., Bai, L., Quin, C., Jing, L., & Fu, H. (2016). Exceptional visible-light-driven cocatalyst-free photocatalytic activity of g-C_3N_4 by well designed nanocomposites with plasmonic Au and SnO_2. *Advanced Energy Materials*, 6(21), 1601190. https://doi.org/10.1002/aenm.201601190

Zada, A., Khan, M., Khan, M. A., Khan, Q., Habibi-Yangjeh, A., Dang, A., & Maqbool, M. J. E. R. (2021). Review on the hazardous applications and photodegradation mechanisms of chlorophenols over different photocatalysts. *Environmental Research*, 195, 110742. https://doi.org/10.1016/j.envres.2021.110742

Zada, A., Khan, M., Qureshi, M. N., Liu, S.-y., & Wang, R. (2020). Accelerating photocatalytic hydrogen production and pollutant degradation by functionalizing g-C_3N_4 with SnO_2. *Frontiers in Chemistry*, 7, 941. https://doi.org/10.3389/fchem.2019.00941

Zada, A., Qu, Y., Ali, S., Sun, N., Lu, H., Yan, R., & Jing, L. (2018). Improved visible-light activities for degrading pollutants on TiO2/g-C3N4 nanocomposites by decorating SPR Au nanoparticles and 2, 4-dichlorophenol decomposition path. *Journal of Hazardous Materials*, 342, 715-723. https://doi.org/10.1016/j.jhazmat.2017.09.005

Zaman, S., Kashif, M., Shah, M., Hameed, A., Majeed, N., Ismail, M., & Khan, N. (2024). Investigating the enhanced photocatalytic degradation of bromophenol blue using Ni/Zn co-doped Strontium oxide nanoparticles synthesized via hydrothermal method. *Brazilian Journal of Science*, 3(1), 102-114. https://doi.org/10.14295/bjs.v3i1.460

Funding

Not applicable.

Institutional Review Board Statement

Not applicable.

Informed Consent Statement

Not applicable.